

Temperature dependence of hyperfine fields at rare-earth nuclei in iron and nickel

H. W. Kugel, L. Eytel,* and G. Hubler†

Department of Physics, Rutgers University, ‡ New Brunswick, New Jersey 08903

D. E. Murnick

Bell Laboratories, Murray Hill, New Jersey 07974

(Received 7 May 1975)

The temperature dependence of the hyperfine fields [$H_0(T)$] at ^{146}Nd and ^{150}Sm nuclei recoil implanted into polarized Fe and Ni were measured from 4 to 650 K with the ion-implantation perturbed-angular-correlation technique. Experimental results for $H_0(4)$ are: FeNd, 3.04(71) MOe; NiNd, 1.67(39) MOe; FeSm, 3.14(35) MOe; NiSm, 1.77(17) MOe. The hyperfine magnetic fields induced at the implanted nuclei by the unquenched orbital angular momentum of the partially filled ionic $4f$ shell [$H_{4f}(T)$] were deduced and the results analyzed in terms of the interactions of the respective rare-earth ionic states with the internal fields of the hosts. Interaction models incorporating pure exchange interactions, exchange and crystal electric field interactions, various implant final-site symmetries, and ionic-excited-state mixing were least-square fit to $H_{4f}(T)$ over various intervals of the observed temperature range. Crystal-electric-field effects are shown to be important in all cases except, perhaps, FeSm. The results of each least-squares-fit analysis are presented and discussed.

I. INTRODUCTION

The unique properties of the lanthanide elements (rare earths) arise from similar outer-electron configurations and an incomplete $4f$ electron shell. Rare-earth compounds typically involve a trivalent state arising from the chemical activity of the outer $6s$ and $5d$ electrons.^{1,2} The stability of this outermost electron configuration gives the rare earths a similar chemical behavior, while the filling of the deep and well-shielded $4f$ shell results in a variety of important optical and magnetic properties. The low-lying energy states of free trivalent rare-earth ions result from spin-orbit splitting of LS -coupled $4f$ electrons into states of fixed total angular momentum (\bar{J}). In bound systems, these states often exhibit a residual splitting due to internal electric and magnetic fields. The additional splitting is characteristic of the nature, intensity, and symmetry of the perturbing fields, and has stimulated many studies of unusual rare-earth compounds and the use of rare earths as probes of internal fields in solids.

The rich variety of phenomena that have been revealed in previous investigations of rare-earth systems continues to motivate new studies of rare-earth ionic level splittings in recently available materials. Ion-implantation techniques, for example, are being used increasingly to bypass the solubility limitations of traditional alloying methods in the preparation of new and unique systems. Rare-earth ions implanted into polarized ferromagnetic transition-metal hosts are especially interesting candidates for investigation, since these systems offer the possibility of displaying

large exchange interactions and a variety of crystal-electric-field effects. The study of such systems may help in the understanding of various rare-earth-host exchange interactions by providing interpretable experimental tests of theoretical models involving a known magnetic impurity interacting with electrons of known state, and by elucidating the origin and nature of crystal electric fields in metals.

This paper reports the results of perturbed-angular-correlation (PAC) measurements of the temperature dependence of the hyperfine fields at ^{150}Sm and ^{146}Nd nuclei recoil implanted into polarized Fe and Ni and the analysis of the results in terms of the interactions of the respective rare-earth ionic ground states with the internal fields of the host. The recoil-implantation PAC technique has the advantage of allowing studies of the splitting of rare-earth ionic states in Fe and Ni using lower concentrations than any other available technique, as well as allowing the use of relatively short nuclear lifetimes. The latter possibility results in simplifying the interpretation of experimental results by limiting the number of observable effects. Potential disadvantages of the recoil-implantation PAC technique are the possibility of radiation-damage effects obfuscating the hyperfine interaction, and the inherent limited precision of the data. However, a considerable body of previous work³⁻⁵ suggests that under controlled conditions radiation-damage effects can be minimized; and the uniqueness and quality of the data obtained are such as to allow meaningful conclusions to be drawn. These studies were undertaken, then, with a view toward understanding new

and unique rare-earth systems that cannot be prepared by conventional alloying methods, to elucidate various nuclear hyperfine interactions, and to provide data for the extension of nuclear-magnetic-moment measurements.

II. EXPERIMENTAL

The basic experimental technique involves the nuclear Coulomb excitation of rare-earth target nuclei to a particular state, and their concurrent recoil implantation into a host lattice, via interaction with high-velocity oxygen projectiles from the Rutgers-Bell tandem Van de Graaff accelerator. The Coulomb excitation of the target nuclei is arranged so as to highly align the spin of the selected nuclear probe and to assure recoil implantation into the host lattice to a maximum depth ($\sim 1.5 \times 10^4 \text{ \AA}$).^{4,5} The implantation is completed in a time ($< 1 \text{ psec}$) short compared to the half-life of the excited nuclear state. In the absence of perturbing fields, the implanted, excited nuclei would remain in their initial highly aligned state. However, this alignment is perturbed by internal electric and magnetic fields. The precession and attenuation of the nuclear alignment is observed by measuring the angular correlation of the γ rays emitted in the decay of the Coulomb excited state.

A 38-MeV $^{16}\text{O}^{8+}$ beam entered the target chamber through an annular surface-barrier particle detector to Coulomb excite nuclei in the enriched targets. The Coulomb-excited nuclei were recoiled into iron or nickel backing foils [Fig. 1(a)]

polarized by a reversible $\sim 2.5\text{-kOe}$ magnetic field. The backscattered-particle counting rate was $\leq 10^3$ particles/sec. γ -ray angular correlations were measured for opposite applied field directions with four movable $7.6 \times 7.6 \text{ cm}^2$ NaI(Tl) crystals mounted on RCA 8854 photomultipliers (at 10 cm) in time coincidence with backscattered ^{16}O ions. Random coincidence events were accumulated simultaneously with true plus random events and subtracted after each run. The coincidence condition helped to insure that detected deexcitation γ rays corresponded to proper implantation and alignment of ^{146}Nd and ^{150}Sm target nuclei in their $J^\pi = 2^+, m=0$ first-excited states. The selective accumulation of γ rays associated with this alignment condition resulted in the observation of highly anisotropic angular correlations. Measurements were made at 12 or more angles at each observation temperature for opposite directions of the applied external polarizing field. The field direction was changed at least once every 5 min to reduce possible systematic effects associated with electronic drift or changes in counting rate. Data were accumulated for a preselected number of backscattered particles, for each external field direction, under computer control. The data acquisition system allowed the various coincidence particle and γ -ray spectra for each field direction to be displayed and monitored during each run. Typical coincidence γ -ray angular correlations for opposite external field directions are shown in Fig. 2.

Measurements were made over two temperature

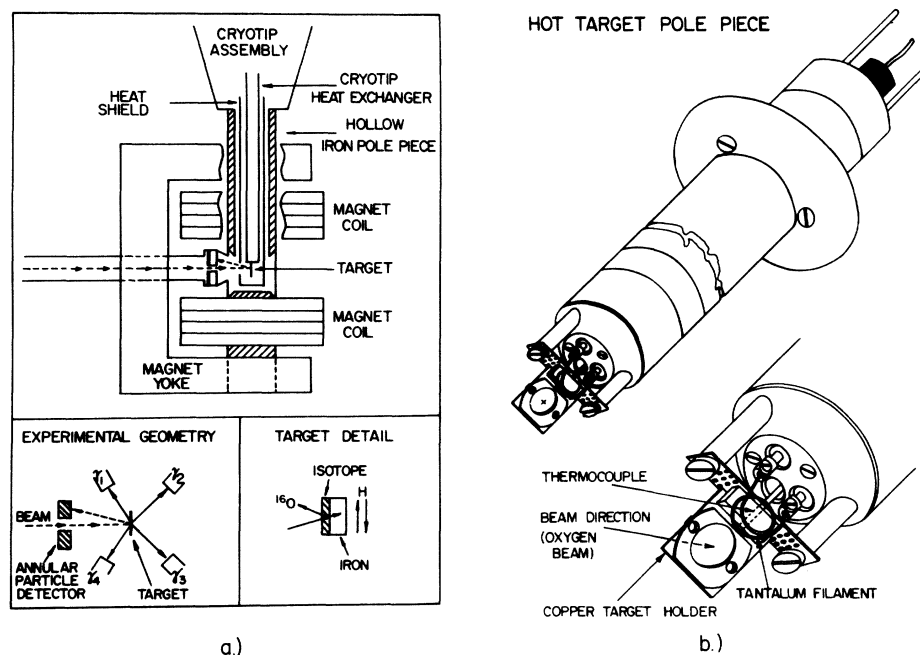


FIG. 1. (a) Schematic diagram of the cold finger and chamber used for the low-temperature measurements and (bottom) general experimental geometry and target detail. (b) Schematic diagram of the hot-target pole piece used for the high-temperature measurements.

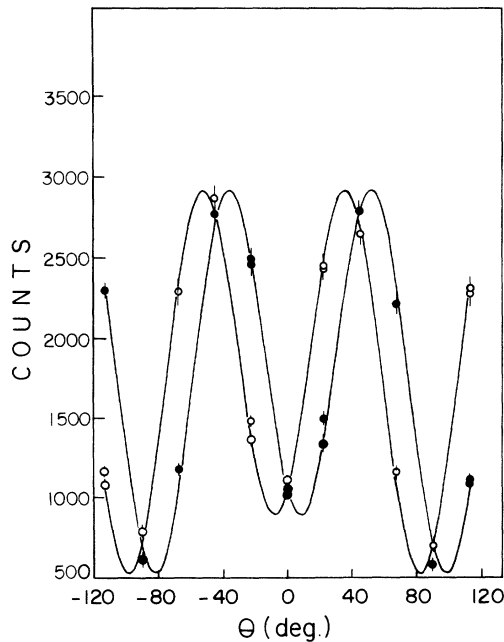


FIG. 2. Typical coincidence γ -ray angular correlation for opposite external field directions (^{150}Sm in Fe at 4.5 K).

ranges (from 2 to 300 K and from 300 to 650 K) using several different targets for each temperature range. Initially, the low-temperature measurements ($T < 300$ K) were made using a Joule-Thompson-effect refrigerator. Subsequent low-temperature measurements were made using a liquid-helium transfer hose to transport liquid helium at a selected rate from a 50-l Dewar to a cold-finger assembly. A resistive sample heater allowed variation of the target temperature. The latter refrigeration method offered greater versatility, convenience, and stability over the entire low-temperature range. A schematic diagram of the experimental apparatus used in the low-temperature measurements is shown in Fig. 1(a). The heat-exchange column used with the liquid-helium transfer hose was held inside a highly reflective nickel-plated heat shield maintained at ~ 20 K. The heat-shield temperature reduced radiative heating of the target and provided a very high cryopumping speed for residual gases in the confined region of the target chamber. The heat-shield and heat-exchanger assemblies were held inside a hollow iron pole piece which was part of the iron electromagnet used for polarizing the ferromagnetic samples. A port in the heat shield allowed the entrance of the accelerated beam and the exit of beam particles backscattered from the target. The targets consisted of 100–400 $\mu\text{g}/\text{cm}^2$ of enriched isotope, vacuum evaporated on 1.27

$\times 10^{-3}$ -cm-thick foils of Fe or Ni. The targets were indium-soldered to the tip of the heat exchanger. The temperature was monitored using a chromel-versus-gold thermocouple mounted at the base of the heat exchanger in thermal contact with a thick copper target holder and mounted approximately 0.5 cm from the 0.16-cm-diam beam spot. The thermocouple output was monitored using a digital microvoltmeter. The target temperature was held constant to within ± 0.5 K. For the beam currents used (a few nanoamps) possible thermal gradients between the beam spot and thermocouple are estimated to be negligible because of the high thermal conductivity of the Fe and Ni foils at low temperatures.

For $T > 300$ K, a specially designed hot-target pole piece [Fig. 1(b)] which provided a field greater than 2.5 kG was employed. The targets were heated in vacuum by radiation from a tantalum filament and temperature was measured by a thermocouple mounted on a copper target holder whose geometry minimized thermal gradients between beam spot and thermocouple. The geometry allowed an estimate of the size of possible thermal gradients, since the temperature was approximately constant throughout the copper (because of its high thermal conductivity) and because of the cylindrical boundary conditions imposed. The gradients were calculated to be of the order of 2 K, and this correction was applied to the thermocouple reading. The fact that this reading was usually constant to within ± 1 K, despite its sensitivity to variations in beam current, is a good indication that such variations were small and that the temperatures assigned were accurate at least to ± 3 K. To help keep the temperature constant, apart from variations in beam current, the entire target holder was insulated from the pole piece with ceramic standoffs and was surrounded by a thin (~ 0.5 mm) copper radiation shield with a port cut in the detection plane to allow for the escape of backscattered oxygen ions. Damage to the surface barrier detector was avoided by mounting it in thermal contact with the beam line and by shielding its front surface with a 6.4×10^{-4} -cm-thick aluminized Mylar foil.

III. ANALYSIS OF THE MEASURED ANGULAR CORRELATIONS

The external polarizing magnetic field was applied perpendicular to the beam axis and to the plane of the γ -ray detectors. For this experimental configuration, the observed γ -ray angular correlation is given by⁶

$$W(\theta) = b_0 + \sum_k \frac{b_k}{[1 + (k\omega\tau)^2]^{1/2}} \cos[k(\theta \pm \Delta\theta)] \quad (1)$$

where $b_0 = 1 + \frac{1}{4}A_2 + \frac{9}{64}A_4$, $b_2 = \frac{3}{4}A_2 + \frac{5}{16}A_4$, $b_4 = \frac{35}{64}A_4$, and $A_k = G_k Q_k A_k$; $k\Delta\theta \approx \arctan(k\omega\tau)$ ($k=2,4$); the arrows refer to the applied field direction. The A_k coefficients are determined by the spins of the initial and final nuclear states and the multipolarity of the γ transition, the Q_k are the geometric attenuation factors due to the finite solid angles of the particle and γ -ray detectors,⁷ and G_k are attenuation factors due to small randomly oriented perturbations. ω is the Larmor precession frequency at τ is the mean lifetime of the excited nuclear state.

The products $\omega\tau$ (the precession angles) were determined by least-squares fitting the observed angular correlations to Eq. (1). The least-squares-fitting procedure was performed by (i) varying $\omega\tau$ while keeping the A_k coefficients fixed at theoretically determined values⁶ and (ii) by varying both $\omega\tau$ and A_k . In all cases the values of $\omega\tau$ derived from both methods were equal to within experimental uncertainties ($\sim 5\%$).

Expect for the case of ^{150}Sm in Ni (NiSm), the values of G_k , as obtained by comparing the A_k coefficients derived from the least-squares-fitting procedure with the calculated theoretical values, were always within experimental uncertainty of $G_k = 1$ over the entire temperature range. This result supports the absence or unimportance of time-dependent relaxation effects that have been observed using longer-lived states in other hosts.⁸⁻¹² The previously observed effects cause the nuclear alignment to decay almost exponentially with time. Several models have been used to interpret these effects in terms of a paramagnetic relaxation of the implanted ion, which speeds up with decreasing temperature.^{13, 14} The present time-integral perturbed-angular-correlation measurements for NiSm cannot reveal the time dependence of the observed attenuations. The apparent

absence of attenuations in the case of NiNd may be due to the much shorter nuclear mean lifetime involved. Future time-dependent perturbed-angular-correlation measurements may be useful for detailed comparisons with various models.

The absence of attenuations in the case of FeSm (body-centered cubic) and their appearance in the case of NiSm (face-centered cubic) suggests the possible relevance of the host crystal lattice structure. Although the distribution of equilibrium sites for many ions recoil implanted in Fe and Ni under various conditions is still under investigation, a variety of studies indicate that for heavier implants under the conditions of these experiments, the predominant final-site distribution is substitutional.^{15, 16} Experimental data for Yb in iron, for example, yields $> 80\%$ substitutional.

IV. ANALYSIS OF THE MEASURED PRECESSION ANGLES

Previous work¹⁷⁻²⁰ has shown that excited nuclei recoil implanted into a polarized ferromagnetic host interact with both static and dynamic hyperfine magnetic fields. The static hyperfine magnetic interaction occurs after the recoiling ion stops. The intensity of the static field (H_0) in most cases is about the same as that of the internal magnetic hyperfine fields acting on nuclei in dilute ferromagnetic alloys, as would be deduced from Mössbauer or NMR measurements. The dynamic hyperfine magnetic interaction occurs as the recoiling ions slow down in the ferromagnetic host prior to stopping. The results of a number of studies indicate that this (transient) field arises from interactions of the magnetic moments of recoil nuclei with polarized electrons in the stopping medium.¹⁷⁻²¹

The impulse nature of the transient field interaction and the resulting small rotation of the an-

TABLE I. Summary of hyperfine field temperature data for Fe^{150}Sm . $H_{\text{cp}}(300) = 0.161$ and $H_{\text{CEP}}(300) = 0.133(13)$ MOe, $g(2+) = 0.273(24)$, and $\tau(2+) = 69.1(1.5)$ psec.

Temperature (K)	$\omega_L\tau_N$ (mrad)	$\omega_L\tau_N - \Delta\phi(T=0)\sigma(T)$ (mrad)	H_0 (MOe)	H_{4f} (MOe)
4.5	-299(17)	-286(20)	3.14(35)	2.84(36)
20	-309(17)	-296(20)	3.25(37)	2.95(38)
77	-304(17)	-291(20)	3.20(36)	2.90(37)
77	-288(16)	-275(19)	3.01(34)	2.71(35)
112.5	-269(16)	-256(19)	2.81(33)	2.51(34)
150	-274(13)	-261(16)	2.87(31)	2.57(32)
200	-253(13)	-240(16)	2.64(29)	2.34(30)
297	-223(6)	-210(9)	2.31(23)	2.02(24)
502	-205(12)	-193(15)	2.12(25)	1.83(26)
553	-170(10)	-158(13)	1.74(21)	1.46(22)
652	-142(9)	-130(12)	1.43(18)	1.16(19)

TABLE II. Summary of hyperfine temperature-dependence data for $Ni^{150}Sm$. $H_{cp}(300) = 0.161$ and $H_{CEF}(300) = 0.036(4)$ MOe, $g(2+) = 0.273(24)$, and $\tau(2+) = 69.1(1.5)$ psec.

Temperature (K)	$\omega_L \tau_N$ (mrad)	$\omega_L \tau_N - \Delta\phi(T=0)\sigma(T)$ (mrad)	H_0 (MOe)	H_{4f} (MOe)
2	-167(5)	-164(6)	1.80(18)	1.60(18)
4	-164(3)	-161(4)	1.77(17)	1.57(17)
20	-157(3)	-154(4)	1.69(16)	1.49(16)
77	-112(5)	-109(6)	1.19(13)	0.99(13)
302	-64(4)	-61(5)	0.67(8)	0.49(9)
427	-43(3)	-40(4)	0.44(6)	0.27(6)
527	-22(2)	-20(3)	0.22(4)	0.08(4)
537	0.0(5)	+ 2(1)	-0.03(1)	-0.16(2)

gular correlation allow the experimentally measured precession angles ($\omega\tau$) to be expressed as

$$\omega\tau \approx \Phi + \omega_0\tau, \quad \omega\tau \approx -g(\Phi/g) - g(\mu_N/\hbar)(H_0\tau), \quad (2)$$

where Φ is the precession angle induced by the transient field interaction, $\omega_0\tau$ is the precession angle induced by the static hyperfine interaction after the recoiling ion stops, g is the g factor of the excited nuclear state, μ_N is the nuclear magneton, and H_0 is the static hyperfine magnetic field.

The reduced transient field precession angles (Φ/g) were calculated for the cases of ^{150}Sm and ^{146}Nd slowing down in Fe and Ni hosts,²¹ and are summarized in Tables I–IV together with the respective nuclear g factors and mean lifetimes adopted in this work. Tables I–IV also include the net hyperfine magnetic fields at the implanted ^{150}Sm and ^{146}Nd nuclei after stopping, as determined from the observed precession angles using Eq. (2).

V. COMPONENT OF THE MEASURED HYPERFINE FIELD OWING TO THE UNQUENCHED ORBITAL ANGULAR MOMENTUM OF THE 4f SHELL

The effective hyperfine magnetic fields at rare-earth nuclei implanted in Fe and Ni can be ex-

pressed as the sum of three effects: (i) Fermi contact interactions involving polarized s electrons associated with an exchange-polarized rare-earth ionic core (core polarization), (ii) Fermi contact interactions involving polarized conduction electrons (conduction-electron polarization), and (iii) the net spin and orbital angular momentum contributions of the partially filled 4f shell. The dominant contribution to the magnitude and temperature dependence of the observed hyperfine fields at Sm and Nd nuclei in Fe and Ni, over most of the observed temperature range, is due to the 4f orbital angular momentum and to the splitting of the rare-earth ionic ground state by the internal fields of the host. The core and conduction-electron polarization and spin dipolar effects result in about 10% contributions to the observed fields. A knowledge of these small contributions is important, however, for an understanding of the behavior of the observed fields at low temperatures. The procedures used to estimate these contributions are discussed below.

A. Hyperfine field owing to core polarization

In the first half of the lanthanide series, the orbital angular momentum (L) of rare-earth impurities in Fe or Ni is aligned antiparallel to the applied field and produces large positive hyper-

TABLE III. Summary of hyperfine field temperature-dependence data for $Fe^{146}Nd$. $H_{cp}(300) = 0.111$ and $H_{CEF}(300) = 0.133(13)$ MOe, $g(2+) = 0.22(4)$, and $\tau(2+) = 31.8(3.2)$ psec.

Temperature (K)	$\omega_L \tau_N$ (mrad)	$\omega_L \tau_N - \Delta\phi(T=0)\sigma(T)$ (mrad)	H_0 (MOe)	H_{4f} (MOe)
4	-102(4)	-93(6)	3.04(71)	2.80(72)
77	-100(3)	-91(5)	2.97(68)	2.73(69)
150	-96(4)	-87(6)	2.84(66)	2.60(67)
301	-81(4)	-72(6)	2.35(56)	2.11(51)
452	-72(5)	-63(7)	2.06(51)	1.83(52)
624	-59(6)	-51(8)	1.67(45)	1.45(46)
652	-57(4)	-49(6)	1.60(41)	1.38(42)

TABLE IV. Summary of hyperfine field temperature-dependence data for $Ni^{146}Nd$. $H_{cp}(300) = 0.111$ and $H_{CEP}(300) = 0.036(4)$ MOe, $g(2+) = 0.22(4)$, and $\tau(2+) = 31.8(3.2)$ psec.

Temperature (K)	$\omega_L \tau_N$ (mrad)	$\omega_L \tau_N - \Delta\phi(T=0)\sigma(T)$ (mrad)	H_0 (MOe)	H_{4f} (MOe)
4	-53(3)	51(3)	1.67(39)	1.52(39)
20	-61(4)	59(5)	1.93(46)	1.78(47)
77	-48(3)	46(3)	1.50(36)	1.36(36)
302	-21(3)	19(3)	0.62(17)	0.48(17)

fine magnetic fields via its magnetic moment. S is antiparallel to L in the first half of the rare-earth series and is therefore parallel to the applied field. The net spin S of the $4f$ shell polarizes the rare-earth ionic core via exchange interactions with core electrons in closed inner shells. Watson and Freeman²² have estimated the strength of this induced hyperfine magnetic field for rare-earth ions as

$$H_{cp} \sim -0.090(g_J - 1)J \text{ MOe}, \quad (3)$$

where g_J is the Landé g factor, J is the total angular momentum of the $4f$ shell, and the term $(g_J - 1)J$ is the projection of S on the J axis. This approximation is believed to be accurate to within (10–20)% and is expected to underestimate the effect slightly as Z increases across the rare-earth series.²² We have adopted Eq. (3) in this work to evaluate the H_{cp} contribution for Sm and Nd. The values of H_{cp} calculated in this manner are $H_{cp}(300) = +0.161$ MOe for Sm and $H_{cp}(300) = +0.111$ MOe for Nd. Very little work has been reported concerning the temperature dependence of H_{cp} . In this work, we assume that the temperature dependence of H_{cp} is identical to that of the host magnetization.

B. Hyperfine field owing to conduction-electron polarization

Conduction-electron polarization (CEP) resulting from exchange mechanisms involving both host and impurity moments produce contributions to the hyperfine magnetic field at impurity nuclei via the Fermi contact interaction. CEP effects provide relatively large negative contributions to the hyperfine magnetic fields observed at transition-metal nuclei in Fe and Ni hosts.²³ The smoothly varying behavior of these fields, and the probable similarity of conduction-electron wave functions in the vicinity of an impurity to the wave functions of its outer bound electrons, have allowed the use of empirical relations to predict H_{CEP} based on the hyperfine field induced by a free atomic ns state.²³

This procedure may not be applicable to rare-earth impurities in Fe and Ni. The antiparallel coupling of L and S by Hund's rule initially sug-

gested an antiferromagnetic coupling between S and the host d electrons and conduction electrons.^{24, 25} Conduction electrons polarized antiparallel to the applied field direction would produce a positive H_{CEP} contribution at the impurity nuclei. Recently, Gomès and Bernas,²⁶ using the results of Campbell,²⁷ have suggested that the conduction-electron magnetization for rare-earth impurities in Fe may be negative. This would give a conduction-electron spin alignment parallel to the applied field and a negative H_{CEP} .

In view of the lack of experimental systematics involving H_{CEP} for rare earths in Fe and Ni, and in view of the theoretical uncertainties, for the purposes of the analysis described below we have estimated the sign and magnitude of H_{CEP} at Sm and Nd nuclei in Fe and Ni hosts using the measured hyperfine magnetic fields at Gd nuclei implanted in Fe at room temperature. The $4f$ shell of Gd^{3+} has zero orbital angular momentum ($L = 0$). In the absence of an orbital magnetic moment, the hyperfine field at Gd nuclei in Fe or Ni was taken as

$$H_0(300) = H_{cp}(300) + H_{CEP}(300). \quad (4)$$

A previous measurement of $H_0(300)$ for Gd gave a value of $-0.200(50)$ MOe.²⁵ We have remeasured the hyperfine magnetic field for this case (using the $4+$ state of ^{156}Gd) and obtain a value of $-0.182(18)$ MOe, in agreement with the previous result. Using Eq. (3) gives $H_{cp}(300) = -0.315$ MOe for Gd (in reasonable agreement with an experimental value of $-0.340(20)$ MOe obtained using other techniques.²⁸ Substituting these values in Eq. (4) gives $H_{CEP}(300) = +0.133(13)$ MOe at Gd nuclei in Fe, and assuming a proportionality to the host bulk magnetic moment gives $H_{CEP}(300) = +0.036(4)$ MOe at Gd nuclei in Ni. In the analysis described below, we have adopted these values for the $H_{CEP}(300)$ of Sm and Nd in Fe and Ni as well. The positive sign for H_{CEP} is consistent with the calculations of Watson and Freeman²⁹ which give a total negative spin density at large distances from the $4f$ shell and support an antiferromagnetic coupling between S and the host magnetization, as implied by the signs of the mea-

sured hyperfine fields at rare-earth nuclei in Fe. An H_{CEP} temperature dependence identical to that of the host magnetization was adopted in the analysis described below.

C. Hyperfine field owing to the 4f shell

The total measured hyperfine magnetic fields (H_0), as given in Tables I–IV, were taken at a given temperature as the sum of the three components discussed above, i.e.,

$$H_0(T) = H_{4f}(T) + H_{\text{cp}}(T) + H_{\text{CEP}}(T), \quad (5)$$

where H_{4f} is the hyperfine field owing to the 4f shell. Values of $H_{4f}(T)$ were obtained as a function of temperature using the relation

$$H_{4f}(T) = H_0(T) - [H_{\text{cp}}(300) + H_{\text{CEP}}(300)] [\sigma(T)/\sigma(300)], \quad (6)$$

where $\sigma(T)$ is the measured³⁰ value of the host magnetization at a given temperature.

VI. ANALYSIS OF 4f HYPERFINE FIELD TEMPERATURE DEPENDENCE

Values of $H_{4f}(T)$ derived in Sec. V are listed in Tables I–IV and are plotted as a function of temperature in Figs. 3–6. The solid and dashed curves represent the results of least-squares fits using various models described below. The values of $H_{4f}(T)$ are normalized to $H_{\text{FI}}(0)$, the free-ion value, which is the calculated hyperfine mag-

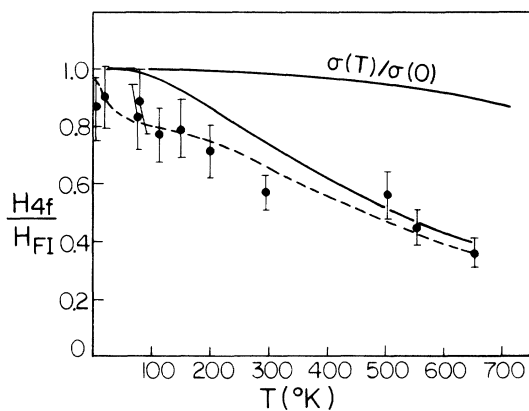


FIG. 3. Deduced values of the 4f hyperfine magnetic field at ^{150}Sm implanted in Fe normalized to the free-ion value H_{FI} vs temperature. The solid line through the data points represents the results of the least-squares fit to the pure exchange model discussed in Sec. VI A. The dashed line represents the results of the least-squares fit to the exchange-plus-crystal-electric-field model discussed in Sec. VI B. The upper solid curve $[\sigma(T)/\sigma(0)]$ illustrates the host magnetization vs temperature.

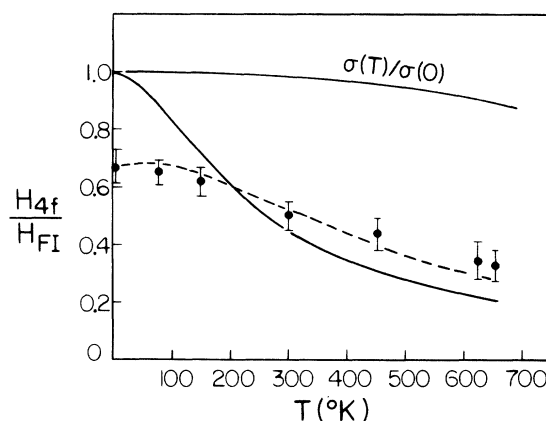


FIG. 4. Results for ^{150}Sm implanted in Ni. See Fig. 3.

netic field³¹ expected at 0 K for a free ion.

We note the following qualitative features of the observed data: (i) In each case, the individual measured values of $H_{4f}(T)$ increase as the temperature decreases until at some low temperature (T_s) a saturation occurs and below this temperature $H_{4f}(T)$ remains approximately constant. This occurs, for example, at about 100 K for FeSm (Fig. 3). (ii) The average saturation values (H_s) of $H_{4f}(T)$ or the projection of H_s onto the ordinate at 0 K usually falls below the free-ion value by about 50%. The exception is the FeSm system, which approaches the free-ion value to within $\sim 10\%$. (iii) The only system that exhibited any attenuation of the perturbed angular correlations was NiSm . In this case magneticlike relaxation attenuations were observed at temperatures ≤ 20 K (Sec. III).

These physical features suggest several possible models which might explain the observations over all or part of the observed temperature range.

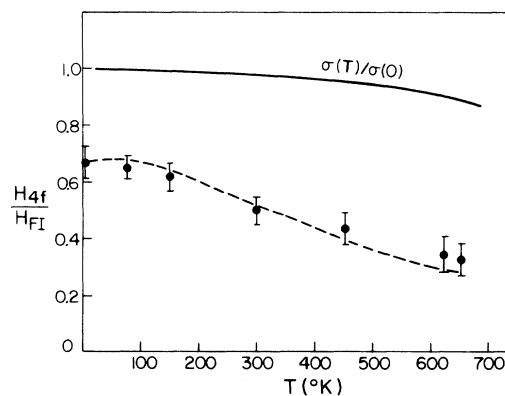


FIG. 5. Results for ^{146}Nd implanted in Fe. See Fig. 3.

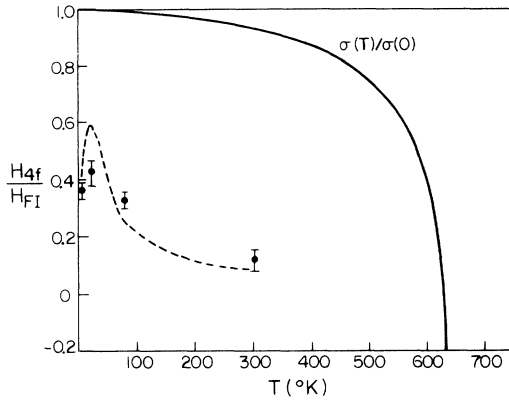


FIG. 6. Results for ^{146}Nd implanted in Ni. See Fig. 3.

A. Simple exchange splitting at temperatures above saturation

The saturation of $H_{4f}(T)$ at a value less than $H_{FI}(0)$ for $T \approx T_s$ is similar to the effects of crystal-electric-field interactions observed in other rare-earth systems (e.g., SmFe garnets³²). Crystal-electric-field interactions become stronger at low temperatures and can be negligible at high temperatures. $H_{4f}(T)$ exhibits a smooth decrease for high temperatures characteristic of a Brillouin-like dependence. Therefore in order to first investigate the extent to which the observed temperature dependencies could be understood in terms of a simple exchange splitting of the rare-earth ionic ground state, the values of $H_{4f}(T)$ for T greater than T_s were least-squares fit to a Brillouin-function temperature dependence. In this simple model, the degeneracy of the ionic ground-state angular momentum (J) is removed by an exchange interaction involving only the S component of J . The exchange energy is

$$E_{\text{ex}} = 2\mu_B(g_J - 1)JH_{\text{ex}}(T), \quad (7)$$

where $H_{\text{ex}}(T)$ is the effective exchange field. The substate population of the split ground state varies with temperature according to a Brillouin function, i.e.,

$$H_{4f}(T) = H_{4f}(0) B_J(X), \quad (8)$$

where $B_J(X)$, with $X = E_{\text{ex}}/kT$ is the Brillouin function for a state of total angular momentum J . The temperature dependence of the exchange field $H_{\text{ex}}(T)$ was taken as identical to that of the host magnetization $[\sigma(T)]$, i.e.,

$$H_{\text{ex}}(T) = H_{\text{ex}}(0) [\sigma(T)/\sigma(0)]. \quad (9)$$

Equation (8) was least-squares fit to $H_{4f}(T)$ at $T > T_s$ for the systems FeSm and FeNd . The amplitude of the Brillouin function $[H_{4f}(0)]$ was set equal to $H_{FI}(0)$, and $H_{\text{ex}}(0)$ (the shape-determining

parameter) was varied. The results are given in Table V and shown as the solid line in Figs. 3–6. In the cases of NiSm and NiNd the available data and low saturation temperatures were such as to not allow this procedure to yield conclusive results.

Table V also includes, for comparison, our similar analysis of data for FeTm based on results of Bernas and Gabriel³³ obtained using an isotope-separator implanted radioactive source and the perturbed-angular-correlation technique to study $H_{4f}(T)$. The impurity doses in this case were much greater than those employed in the present work, thus possibly being subject to greater dose and radiation-damage effects.

The values of $H_0(T)$ given in Tables I–IV were also least-squares fit directly in an attempt to fit $H_{\text{cp}} + H_{\text{CEP}}$, as well as $H_{4f}(T)$ as given in Eq. (6). The results for the fitted value of $H_{\text{cp}} + H_{\text{CEP}}$ were unphysical based on previous arguments and the overall fit was not improved conclusively.

In the cases of FeSm and NiSm , the effect of the exchange mixing, at higher temperatures, of the first-excited ionic state ($J = \frac{7}{2}$) of the Sm^{3+} ion (1100 cm^{-1} above the ground state) was also investigated. $H_{4f}(T)$ for FeSm and NiSm was least-squares fit for the temperature dependence resulting from exchange mixing of the $J = \frac{7}{2}$ state. The ground-state wave function which includes the exchange mixing of the $J = \frac{7}{2}$ state, in first-order perturbation theory, is

$$\begin{aligned} \psi_{\text{gs}}(M) = \psi(J = \frac{5}{2}, M) + \left(\frac{2(g_{5/2} - 1)}{g_{5/2}} \mu_B H_{\text{ex}} \langle \frac{7}{2} \| \vec{L} \| \frac{5}{2} \rangle \right. \\ \left. \times \frac{[(\frac{7}{2})^2 - M^2]^{1/2}}{E_{5/2, M} - E_{7/2, M}} \psi(J = \frac{7}{2}, M) \right), \end{aligned} \quad (10)$$

where the reduced matrix elements have been tabulated for all rare-earth 3^+ ions by Elliott and Stevens.² The temperature dependence of $H_{4f}(T)$ is given by the thermal average over all substates,

$$H_{4f}(T) = H_{4f}(0) \frac{\sum_M \langle \psi_{\text{gs}}(M) | N_Z | \psi_{\text{gs}}(M) \rangle e^{-E_{5/2, M}/kT}}{\sum_M e^{-E_{5/2, M}/kT}}, \quad (11)$$

TABLE V. Pure exchange splitting for $T > T_s$.

Host: impurity	Fitted $H_{\text{ex}}(0)$ (MOe)
FeNd	-2.28(19)
FeSm	-2.78(20)
FeTm ^a	-1.20(3)

^a From Ref. 33. See text.

where N_Z is a hyperfine operator defined by Elliott and Stevens.² This procedure yielded results which appeared to slightly improve fits to data at high temperatures but did not improve the quality of the fits to data extending over the entire temperature range.

B. Exchange and crystal-electric-field splitting over entire temperature range

In the case of pure exchange splitting, the ionic ground-substate population reaches a distribution at $T=0$ K for which $H_{Af}(0) = H_{FI}(0)$. The presence of an electric field at the impurity site in the host lattice can produce additional splitting. This effect becomes strongest at $T=0$ K and results in a saturation of $H_{Af}(0)$ at less than $H_{FI}(0)$. With the exception of $FeSm$, the systems studied in this work exhibit a low-temperature saturation of $H_{Af}(T)$ which is substantially less than $H_{FI}(0)$, suggesting the presence of additional splitting due to crystalline electric fields (CEFs).

In order to investigate the influence of CEF splitting, $H_{Af}(T)$ was least-squares fit to a function which included both exchange and electric field interactions. The interaction Hamiltonian (\mathcal{H}) was written

$$\mathcal{H} = E_{ex}(H_{ex}) + V_{el}(q), \quad (12)$$

where $E_{ex}(H_{ex})$ is the exchange energy described above and $V_{el}(q)$ is the CEF potential. A point-charge model was used as a first-order approximation to $V_{el}(q)$. Previous applications of this model³⁴ to rare-earth-metallic systems have indicated inconsistencies between CEF field strengths predicted *a priori* by the model and field strengths derived from its use in the analysis of experimental data. The computational simplification resulting from attributing the CEF at the impurity to effective point electric charges on nearest-neighbor lattice ions results in neglecting possibly important aspects of the interaction, such as the actual lattice ion and conduction-electron charge distributions and various shielding, polarization, and overlap effects involving electrons of the impurity and host. However, in view of the complexities of the complete interaction, the theoretical uncertainties, and the limits of the experimental data, the use of a Hamiltonian based on the point-charge description having the correct symmetry is a reasonable parametrization convenient for comparative studies. Such an analysis can help to determine the strengths of at least lower-order CEF terms from the experimental data available.

The operator-equivalents method of Stevens³⁵ was used for evaluating the matrix elements of

the crystalline potential between substates of a particular angular momentum J . The explicit form of the exchange-plus-CEF Hamiltonian is

$$\mathcal{H} = [2\mu_B(g_J - 1)\vec{J} \cdot \vec{H}_{ex}] + [B_4(O_4^0 + 5O_4^0) + B_6(O_6^0 - 21O_6^4)], \quad (13)$$

where the O_k^j 's are operator equivalents of matrix elements within a given J manifold. The coefficients B_4 and B_6 for different cubic coordinations are given by Hutchings.³⁶ The numerical results of Hutchings³⁶ were used to complete the evaluation of the matrix elements. An eightfold cubic symmetry of point charges (with charge q) was used to describe $V_{el}(q)$ at an implant having a substitutional site in the bcc lattice of the Fe host and a 12-fold cubic symmetry was used to describe $V_{el}(q)$ at an implant having a substitutional site in the fcc lattice of the Ni host. The charges q reside on nearest-neighbor lattice sites, and since $\langle r^4 \rangle_{Af}$ and $\langle r^6 \rangle_{Af}$ are not expected to vary greatly for Nd^{3+} and Sm^{3+} , the CEF model in its simplest form would imply equal q in a given host. The customary procedure, however, is to regard either B_4 and B_6 , or q for different coordinations, as parameters to be fitted. The temperature dependence of the interaction that was used to least-squares fit $H_{Af}(T)$ over the entire temperature range is

$$H_{Af}(T) = H_{FI}(0) \langle N_Z \rangle, \quad (14)$$

where $\langle N_Z \rangle$ is the thermal average of N_Z . $H_{ex}(0)$ was varied as a free parameter. The results are given in Table VI and are shown by the dashed curves in Figs. 3–6. Crystalline-electric-field contributions to the splitting of the ionic ground states appear to explain the observed lower saturation values of $H_{Af}(0)$. In addition, crystalline-electric-field effects seem to improve the fits at high temperatures by requiring a lower value of $H_{ex}(0)$. For completeness, Table VI also includes the results of a similar analysis of the data of Bernas and Gabriel³³ for $FeTm$.

The effect of first-excited-state ($J = \frac{7}{2}$) mixing of Sm^{3+} was also investigated for cases of exchange and crystalline-electric-field splitting. The results did not indicate a conclusive improvement of the least-squares fits over those using only a ground-state splitting.

Recently deWijn and co-workers^{37, 38} have discussed the use of strong J mixing to explain the temperature-dependent magnetic properties of Sm^{3+} in various CEF systems. The three lowest J multiplets were used in their analysis. This gave a nonzero sixth-order term, rather than just a fourth-order term as in the case when only the $J = \frac{5}{2}$ ground state is used. This procedure was

TABLE VI. Fitted exchange-plus-crystalline-electric-field parameters.

Host: implant	q (a.u.)	H_{ex}	χ^2	B_4	B_6	Exchange mixing
<i>FeNd</i>	-5.0(5)	-0.185(3) a.u. =-3.16(5) MG	0.67	$-5.39(54) \times 10^{-7}$ a.u. =-0.17(2) K	$4.43(44) \times 10^{-9}$ a.u. =0.0014(1) K	No
<i>NiNd</i>	+0.99(2)	-0.029(3) a.u. =-0.50(5) MG	9.82	$3.34(50) \times 10^{-7}$ a.u. =0.10(2) K	$-1.33(20) \times 10^{-8}$ a.u. =-0.0040(6) K	No
<i>FeSm</i>	+3.69(67)	-0.151(15) a.u. =-2.58(26) MG	0.58	$294(53) \times 10^{-6}$ a.u. =0.92(16) K		No
<i>NiSm</i>	+1.37(40)	-0.025(4) a.u. =-0.43(7) MG	0.19	$3.14(1.02) \times 10^{-6}$ a.u. =0.99(32) K		Yes $T > 500$ K
<i>FeTm</i> ^a	+0.65(22)	0.069(002) a.u. =1.18(3) MG	1.91	$1.71(58) \times 10^{-8}$ a.u. =0.005(2) K	$2.51(85) \times 10^{-8}$ a.u. =7.9(2.7) $\times 10^{-6}$ K	No

^a From Ref. 33. See text.

applied³⁸ in a preliminary manner to the data presented in this work and yielded a physically realistic range of values for the strengths of B_4 and B_6 , which included within experimental uncertainties the field strengths derived using only fourth-order fields as described above and shown in Table VI. The present experimental resolution is not sufficient to resolve the effects of excited-state mixing for the *FeSm* system.

VII. DISCUSSION

The models used in this work to analyze the temperature dependence of $H_{4f}(T)$ may be summarized as follows: (a) pure exchange splitting for $T > T_s$, forcing $H_{4f}(T=0) \rightarrow H_{\text{FI}}$, and (b) exchange plus point-charge cubic crystal field over the entire temperature range, making no initial assumptions about the relative influence of CEF versus pure exchange on the $4f$ splitting [and thus $H_{4f}(T)$] at $T=0$. Each of these models is a limiting case of the real physical system, yet the qualitative and quantitative features of the data parametrization with these models has helped to elucidate the relevant physics and suggest areas of future research.

The exchange-plus-crystal-field model (b) yields good fits to the data, but also provides a physical explanation for the saturation of $H_{4f}(T \rightarrow 0)$ in terms of CEF. Moreover, the H_{ex} derived from model (b) agree within errors with those derived from model (a) for *FeTm*, *FeSm*, and *FeNd* (Tables V and VI). This implies that CEF effects are important mainly at low temperatures, and that fits to model (b) derive H_{ex} mostly from the higher-temperature ($T > T_s$) data. In this sense, model (a) is really a limiting case of model (b) and is useful as a consistency check. The assumption

of substitutional sites for *FeSm* (eightfold coordination) gave excellent least-square fits to Eq. (14), with physically reasonable values for q . Previous CEF studies have yielded conservation of the sign of q for a given rare earth in various hosts.^{34,39} Applying conservation of q in the present work yields excellent least-square fits for substitutional *NiSm* (12-fold coordination) and very poor least-square fits for body-centered interstitial (sixfold coordination) *NiSm*. The least-squares analysis of the *NiSm* was improved using exchange mixing for $T > 500$ K and Eq. (14) for $T < 500$ K. Since it was unnecessary to invoke exchange mixing for *FeSm* where H_{ex} is much larger, some other effect may be responsible for the decrease in the *NiSm* field above 500 K. Similarly, the assumption of substitutional sites for *FeNd* (eightfold cubic coordination) yielded excellent least-square fits of Eq. (14) to $H_{4f}(T)$. Variation of the B_4/B_6 ratio decreased the quality of least-square fits. The analysis of the *NiNd* results was significantly improved assuming substitutional sites of 12-fold coordination rather than sixfold and eightfold coordinates.

The variation in the sign of q from one metallic host to another has been observed previously for Nd impurities.⁴⁰ However, the relatively poor quality of the best fit to the *NiNd* data shown in Fig. 6 indicates that either the simple-exchange-plus-crystal-field model is less appropriate for this system (possibly because of additional effects, such as a distribution of final sites and radiation-damage effects) or that improved experimental resolution of the observed temperature dependence is required. The relatively small temperature dependence due to low saturation values of $H_{4f}(T)$ and smaller precession angles contributes to the experimental difficulties involved in precession

measurements of the temperature dependence for Ni systems. In addition, for NiNd, the uncertainty in the ^{146}Nd g factor (15%) and the estimated errors in $H_{\text{cp}} + H_{\text{CEP}}$ resulted in relatively larger uncertainties in $H_{4f}(T)$ for all temperatures.

The fitted CEF strengths for all cases studied are comparable to those derived by Williams and Hirst³⁴ from susceptibility data on AuR and AgR solid solutions ($B_4/\beta_{\text{max}} \approx 70$ K) and are of the same order as those found for praseodymium calco-genides and pnictides by Tuberfield *et al.*³⁹ using neutron scattering ($B_4/\beta_{\text{max}} \approx 150$ K), if one takes into account the differences in $\langle r^4 \rangle_{4f}$, $\langle r^6 \rangle_{4f}$, and nearest-neighbor distances used to calculate the relevant parameters.

The exchange fields (H_{ex}) derived using model (b) for the Fe hosts are in good agreement with those derived assuming a simple exchange splitting for $T > T_s$ [model (a)]. In addition, the coordinations for best fits with model (b) corroborate the assumption of substitutional implants (Sec. III).

Table VII gives ratios of total hyperfine fields [$H_0(4.2)$] at Nd and Sm nuclei in various systems to the respective free-ion fields [$H_{\text{FI}}(0)$]. The values for the implanted FeNd, FeSm, and NiNd systems are comparable within experimental uncertainties to similar trivalent metallic compounds. However, the NiSm ratio is about a factor-of-2 smaller than the value for FeSm and other metallic Sm compounds. This appears consistent with the possible relaxation effects discussed above in relation to the observed finite PAC attenuations at $T < 20$ K and the behavior of $H_{4f}(T)$ in the case of NiSm.

The analysis of the present results exhibits sufficient sensitivity to the expected crystal-field

TABLE VII. Comparison of hyperfine magnetic fields [$H_0(4.2)$] at Nd and Sm nuclei in various systems with the respective free-ion fields [$H_{\text{FI}}(0)$].

System	H_0/H_{FI}	System	H_0/H_{FI}
FeNd ^a	0.72(17)	FeSm ^a	0.95(11)
NiNd ^a	0.40(9)	NiSm ^a	0.54(5)
NdAl ^b	0.82(1)	SmFe ₂ ^c	0.95(5)
NdCo ₂ ^b	0.83(2)	SmNi ^c	0.95(10)
NdRu ₂ ^b	0.55(2)	SmAl ₂ ^c	1.03(5)
NdIr ₂ ^b	0.50(2)	Sm ^c	1.01(5)
NdNi ₂ ^b	0.55(2)	SmIG ^c	0.84(5)

^a Present work.

^b See Ref. 40.

^c See Ref. 41.

symmetries to suggest the usefulness of additional studies of similar systems in elucidating the relative importance of exchange and electrostatic interactions for rare earths in simple ferromagnetic hosts. The behavior of $H_{4f}(T)$ near $T=0$ yields the most information on the CEF interaction, whereas results near the Curie point yield information about the exchange field under the assumption that $H_{\text{ex}}(T) = H_{\text{ex}}(0)\sigma(T)$. In addition, a measurement of $H_0(T)$ for FeGd³⁺ (see Sec. VB) should yield a better understanding of the relative importance of the two components of H_{CEP} for the rare earths in metallic ferromagnets, and would aid in any reanalysis of the present results.

ACKNOWLEDGMENTS

Helpful discussions with many of our colleagues are appreciated. In particular, the comments and calculations of H. deWijn were of significant value.

*Present address: Atomics International Inc., Canoga Park, Calif. 91403.

†Present address: Naval Research Laboratory, Washington, D. C.

‡Work supported in part by the National Science Foundation.

¹J. W. Van Vleck, *The Theory of Electric and Magnetic Susceptibilities*, (Oxford U. P., London, 1932).

²R. J. Elliott and K. W. H. Stevens, Proc. R. Soc. A **218**, 553 (1953).

³L. Grodzins, in *Nuclear Reactions Induced by Heavy Ions*, edited by R. Bock and W. R. Hering (North-Holland, Amsterdam, 1970).

⁴R. R. Borchers, in *Hyperfine Interactions in Excited Nuclei*, edited by G. Goldring and R. Kalish (Gordon and Breach, New York, 1971), p. 31.

⁵L. Eytel, P. Raghavan, D. E. Murnick, and R. S. Raghavan, Phys. Rev. B **11**, 1160 (1975).

⁶H. Frauenfelder and R. M. Steffen, in *Alpha- Beta- and*

Gamma-Ray Spectroscopy, edited by K. Siegbahn (North-Holland, Amsterdam, 1965), Vol. 2, p. 997.

⁷M. Yates, in *Perturbed Angular Correlations*, edited by E. Karlsson, E. Matthias, and K. Siegbahn (North-Holland, Amsterdam, 1964), p. 453.

⁸R. Stiening and M. Deutsch, Phys. Rev. **121**, 1484 (1961).

⁹M. E. Caspari, S. Frankel, D. Ray, and G. T. Wood, Phys. Rev. Lett. **6**, 345 (1961).

¹⁰D. W. Gebbie, C. Scherer, D. L. Heeber, G. M. Heestand, and R. R. Borchers, Phys. Rev. B **7**, 4821 (1973).

¹¹P. Ryge, H. W. Kugel, and R. R. Borchers, in Ref. 4, p. 1043.

¹²J. C. Waddington, K. A. Hagemann, S. Ogaza, D. Kiss, B. Herskind, and B. I. Deutch, in *Nuclear Reactions Induced by Heavy Ions*, edited by R. Bock and W. R. Hering (North-Holland, Amsterdam, 1970), p. 438.

¹³M. Blume, in *Hyperfine Structure and Nuclear Radiations*, edited by E. Matthias and D. A. Shirley (North-

- Holland, Amsterdam, 1968), p. 427.
- ¹⁴A. Abragam and R. V. Pound, *Phys. Rev.* **92**, 943 (1953).
- ¹⁵H. de Waard and L. C. Feldman, in *Application of Ion Beams to Metals*, edited by S. T. Picraux, E. P. Eernisse, and F. L. Vook (Plenum, New York, 1974), p. 317.
- ¹⁶L. C. Feldman, E. N. Kaufmann, D. W. Mingay, and W. M. Augustyniak, *Phys. Rev. Lett.* **27**, 1145 (1971).
- ¹⁷R. R. Borchers, B. Herskind, J. Bronson, L. Grodzins, R. Kalish, and D. Murnick, *Phys. Rev. Lett.* **20**, 424 (1968).
- ¹⁸R. R. Borchers, J. Bronson, D. Murnick, and L. Grodzins, *Phys. Rev. Lett.* **17**, 1099 (1966).
- ¹⁹G. M. Heestand, R. R. Borchers, B. Herskind, L. Grodzins, P. Kalish, and D. E. Murnick, *Nucl. Phys. A* **133**, 310 (1969).
- ²⁰J. Lindhard and A. Winther, *Nucl. Phys. A* **166**, 413 (1971).
- ²¹G. K. Hubler, Ph.D. thesis (Rutgers University, 1972) (unpublished); G. K. Hubler, H. W. Kugel, and D. E. Murnick, *Phys. Rev. C* **9**, 1954 (1974).
- ²²R. E. Watson and A. J. Freeman, in *Hyperfine Interactions*, edited by A. J. Freeman and R. B. Frankel (Academic, New York, 1967).
- ²³D. A. Shirley, S. S. Rosenblum, and E. Matthias, *Phys. Rev.* **170**, 363 (1968).
- ²⁴F. Boehm, G. Hagemann, and A. Winther, *Phys. Lett.* **21**, 217 (1966).
- ²⁵L. Grodzins, R. Borchers, and G. Hagemann, *Phys. Lett.* **21**, 214 (1966).
- ²⁶A. A. Gomès and H. Bernas, *Phys. Lett. A* **39**, 202 (1972).
- ²⁷I. A. Campbell, *J. Phys. C* **2**, 1338 (1969).
- ²⁸S. Hüfner, *Phys. Rev. Lett.* **19**, 1034 (1967), and references therein.
- ²⁹R. E. Watson and A. J. Freeman, *Phys. Rev. Lett.* **6**, 277 (1961).
- ³⁰J. Crangle and G. M. Goodman, *Proc. R. Soc. A* **321**, 477 (1971).
- ³¹See Ref. 2. $H_{F1}(\text{Sm}) = 3.3 \text{ MG}$, $H_{F1}(\text{Nd}) = 4.2 \text{ MG}$.
- ³²S. Ofer, E. Segel, I. Nowick, E. R. Bauminger, L. Grodzins, A. J. Freeman, and M. Schieber, *Phys. Rev.* **137**, A627 (1965).
- ³³H. Bernas and H. Gabriel, *Phys. Rev. B* **7**, 468 (1973).
- ³⁴G. Williams and L. L. Hirst, *Phys. Rev.* **185**, 407 (1968).
- ³⁵K. W. H. Stevens, *Proc. Phys. Soc. A* **65**, 209 (1952).
- ³⁶M. T. Hutchings, in *Solid State Physics*, edited by F. Seitz and D. Turnbull (Academic, New York, 1964), Vol. 16, p. 227.
- ³⁷H. W. deWijn, A. M. van Diepen, and K. H. J. Buschow, in *Proceedings of the Conference on Crystalline Electric Field Effects in Metals and Alloys*, Montreal, Canada, June, 1974 (unpublished).
- ³⁸H. W. deWijn (private communication).
- ³⁹R. C. Turberfield, L. Passell, R. J. Birgeneau, and E. Bucher, *Phys. Rev. Lett.* **25**, 752 (1970).
- ⁴⁰G. Kaindl, *Z. Phys.* **240**, 100 (1970).
- ⁴¹S. Ofer and I. Nowik, *Nucl. Phys. A* **93**, 689 (1967).